Chemical Engineering Journal 156 (2010) 404–410

Contents lists available at ScienceDirect

Chemical Engineering Journal

journal homepage: www.elsevier.com/locate/cej

Effects of nitrogen doping on the structure of carbon nanotubes (CNTs) and activity of Ru/CNTs in ammonia decomposition

Jiuling Chen [a], Zhong Hua Zhu [a,*], Shaobin Wang [b,**], Qing Ma [a], Victor Rudolph [a], Gao Qing Lu [c]

[a] Division of Chemical Engineering, School of Engineering, The University of Queensland, St Lucia, QLD 4072, Australia
[b] Department of Chemical Engineering, Curtin University of Technology, GPO Box U1987, Perth, WA 6845, Australia
[c] ARC Centre of Excellence for Functional Nanomaterials, The University of Queensland, Brisbane, QLD 4072, Australia

ARTICLE INFO

Article history:
Received 24 April 2009
Received in revised form 25 October 2009
Accepted 30 October 2009

Keywords:
Microwave plasma
Nitrogen doping
CNT-supported Ru catalyst
Ammonia decomposition
Hydrogen production

ABSTRACT

Nitrogen doping on carbon nanotubes (CNTs) was carried out using N_2 microwave plasma at the powers of 200 and 400 W. N_2 physisorption, XPS, XRD, TEM, and CO chemisorption were employed to investigate the effects of nitrogen doping on the structure of CNTs and the state of Ru particles supported on CNTs. The bulk structure and the surface texture of CNTs remain unchanged by such nitrogen doping. Two types of nitrogen species, pyridinic and quaternary nitrogen, were found on the surface of nitrogen doped CNTs. Pyridinic nitrogen atom may have a strong interaction with Ru. The average Ru particle size decreases with the increase of pyridinic nitrogen content. The activity of Ru/CNTs catalysts in ammonia decomposition is dependent on the dispersion of Ru particles and remaining nitrogen on the surface of CNTs.

1. Introduction

Proton-exchange membrane fuel cells are expected to replace traditional internal combustion engines in the future to reduce exhaust emissions and improve efficiency. The supply of fuel hydrogen and sufficient energy storage on vehicles, in particular, become a challenge, with one potential solution being the on-board hydrogen production [1,2]. The current mainstream processes for hydrogen production such as steam reforming or autothermal reforming of hydrocarbons have limited application because they produce some CO, which poisons the noble metal electrodes even at CO concentration as low as 10 ppm [3–6]. Suitable cleanup equipment to completely remove CO after reforming is difficult to achieve for on-board hydrogen production. As an alternative route for hydrogen supply, catalytic decomposition of ammonia eliminates the generation of CO while retaining the advantage of storing hydrogen in high energy density form of liquid ammonia. The small amount of the unconverted ammonia that passes through decomposition reactor can be decreased to less than 200 ppb using an effective absorber [1,2,6–11].

It is known that Ru catalysts show higher activity in ammonia decomposition compared with other common metal catalysts such as Fe, Ni, Pd, Pt and Rh. It is also known that the activity is dependent on the nature and the structure of support materials [2,6–11]. Some investigations have shown that carbon nanotubes (CNTs) exhibit higher activity of Ru catalysts than activated carbon, Al_2O_3, TiO_2, MgO and ZrO_2 [9,10]. The reason is believed to be related with easier electron transfer from CNTs to Ru particles due to the good electronic conductivity of CNTs, which can induce a decreased ionization potential of Ru favoring the desorption of adsorbed nitrogen atoms on Ru surface [9,10,12–16]. On the other hand, single crystal studies and DFT calculations indicate that the process of N_2 desorption is a structure sensitive reaction and relates to the ensembles of five Ru atoms (B_5-type active sites) on the surface of Ru particles [15,16]. The maximum probability for B_5-type active sites occurring is at 1.8–2.5 nm of Ru particles and larger particle will result in the probability monotonically decreasing [16]. Therefore, the activity of Ru/CNTs in ammonia decomposition can be promoted via improvement of electron transfer of CNTs or the dispersion of Ru particles.

The surface of primitive CNTs is inert and few anchor sites are available for Ru particles. However, pretreatment with strong oxidants will produce oxygen-containing groups on the surface of CNTs, especially phenolic hydroxyls and carboxyls, which can act as effective sites for binding to obtain the highly dispersed Ru particles [10,17]. Since these groups are chemically and strongly bounded with carbon, some oxygen-containing groups still remain on Ru/CNTs after reduction in hydrogen and the electron-withdrawing effects, which are more electronegative than Ru, are disadvantageous to the activity of Ru particles [9,10,12–16]. In contrast

* Corresponding author.
** Corresponding author. Tel.: +61 8 9266 3776; fax: +61 8 9266 2681.
E-mail addresses: z.zhu@uq.edu.au (Z.H. Zhu), shaobin.wang@curtin.edu.au (S. Wang).

1385-8947/$ – see front matter © 2009 Elsevier B.V. All rights reserved.
doi:10.1016/j.cej.2009.10.062

to oxygen groups, some surface nitrogen-containing groups, e.g. –C–N=C–, can anchor Ru particles as well and can be more easily removed during hydrogen reduction [12].

In this work, N_2 microwave (MW) plasma was employed for nitrogen doping on the surface of CNTs. The influence of the doping on the structure of CNTs was studied using X-ray photoelectron spectroscopy (XPS), X-ray diffraction (XRD), and N_2 physisorption. The state of Ru particles was observed with a transmission electron microscope (TEM) and CO chemisorption. The activity of Ru/CNTs in ammonia decomposition to produce hydrogen was measured in a fixed-bed reactor.

2. Experimental

2.1. Doping of nitrogen and loading of Ru on CNTs

CNTs, produced from methane decomposition over Fe catalysts in a fluidized-bed reactor, were supplied by Tsinghua University, China and the purity in the primitive samples was above 95%. The orientation of the carbon layers in a typical CNT is parallel to its axis. The external diameter of CNTs is in the range of 10–30 nm and most of CNTs have the diameter around 20 nm. The inner diameters are typically about one third of the corresponding external diameters. After synthesis, CNTs were soaked in 4 M HNO_3 solution at room temperature for 24 h to remove Fe particles and then washed with water to neutrality. After cleaning, CNTs were dried in air at 393 K for 5 h and sieved into different size fractions. The particles of 63–500 μm were used for N-doping experiments.

Nitrogen doping in N_2 MW plasma was carried out in a vertical quartz tube, which had an internal diameter of 46 mm and was located inside MW waveguide cavity. MW was generated from a magnetron with power of 50–1000 W and a fixed frequency 2.45 GHz. Detailed information about the equipment can be found elsewhere [18]. An infrared transducer was employed to monitor the temperature of CNTs. Approximately 1.0 g CNTs was used for each experiment which was exposed for 5 min under N_2 at a flow rate 120 ml min^{-1} (STP) and pressure 60–90 Torr. Samples were produced at MW powers of 200 or 400 W and the corresponding reflected powers were 2–3 W. The samples obtained were denoted as follows: CNT-un (undoped CNT samples), CNT-200 (doped at 200 W) and CNT-400 (doped at 400 W).

The loading of Ru on CNTs was carried out by an impregnation method with aqueous solution of $RuCl_3$. The loading contents of Ru on CNTs were 0.8 wt.%. After loading, the samples were dried for 24 h in air at room temperature and then calcined in a quartz tube under N_2 at a heating rate of 2 K min^{-1} from ambient to 773 K and at 773 K for 10 h.

2.2. Characterization

The binding energies (BEs) of N1s and the elemental composition of CNTs samples before and after nitrogen doping were measured with a PHI-560 ESCA system Perkin-Elmer XPS. The binding energy values were corrected by taking C1s, 284.5 eV, as a criterion. All spectra were acquired at a pressure 2×10^{-7} Torr with Mg Kα excitation at 15 kV.

The XRD profiles of CNTs before and after nitrogen doping were obtained on a Bruker D8 advanced research XRD with Cu Kα radiation at a scanning rate of 2° min^{-1}.

The pore structures of CNTs were measured using N_2 physisorption on a NOVA 1200 adsorption analyzer (Quantachrome). Specific surface areas of the samples were obtained from the BET equation. The pore size distribution of the samples was evaluated by the desorption branch of the isotherm.

The Ru particles of Ru/CNTs after reduction in hydrogen at 773 K were observed with a JEOL JEM 1010 TEM. The Ru/CNTs samples were also investigated with XPS instrument under the same conditions as described above.

CO chemisorption at room temperature was employed to measure the dispersion and the average size of Ru particles on Ru/CNTs samples in a conventional pulse system. The samples were first reduced in flowing hydrogen at 773 K for 2 h and then followed by flushing for 2 h in a helium stream of 50 ml min^{-1} at 773 K with subsequent cooling in flowing helium to ambient temperature. CO pulses (200 μl each one) were injected into the helium carrier gas and detected by TCD. By comparing the amount of CO reaching the detector and the amount of CO injected, the quantity of CO adsorbed could be determined. Blank experiments on CNT showed there was no measurable uptake of CO on the support itself.

2.3. Ammonia decomposition

In ammonia decomposition reaction, 100 mg catalyst samples were used for each experiment. A vertical quartz tube reactor with an inner diameter of 8 mm was used. The catalyst was first heated in hydrogen to 773 K at a heating rate of 5 K min^{-1} and then held at 773 K for 2 h to reduce the Ru catalyst. Finally the temperature was adjusted to the required value and the feed was switched from hydrogen to argon to flush the system for 30 min and then switched to ammonia for the decomposition reaction. Ammonia with a flow rate of 70 ml min^{-1} (STP) was used as reactant. All the reactions were performed at atmospheric pressure. A Shimadzu GC-8A gas chromatograph equipped with a TCD was employed to measure the composition of product gas. Argon was used as the carrier gas.

3. Results

During the process of nitrogen doping on CNTs in N_2 MW plasma, the color of the plasma flame was pink and the plasma light became brighter with increasing MW power. The temperatures of the CNT samples during the doping process were around 1063 K (790 °C) and 1213 K (940 °C), respectively, at the MW power of 200 and 400 W.

3.1. Characterization of CNTs

Fig. 1 presents the XPS survey scans of CNT-un, CNT-200 and CNT-400. The spectra show stronger carbon signal than nitrogen. However, the nitrogen peak is clearly observed in the XPS spectra for CNT-200, while it is very weak for CNT-400 and cannot be discerned for CNT-un. The results of elemental analysis are listed in Table 1. The nitrogen content of CNT-un, CNT-200 and CNT-400 is quite different. CNT-200 gives the highest value and CNT-un shows the lowest, CNT-400 gives the intermediate value. For oxygen content, CNT-200 and CNT-400 exhibit similar but much reduced oxygen concentration compared with CNT-un, which is due to the treatment of samples at high temperatures. The content of Fe on the three CNT samples is all around 0.05%, which suggests

Table 1
Elemental analysis of CNT samples and reduced Ru/CNTs.

Samples	Elemental content (%)				
	C	N	O	Fe	Others (Si, Ca, Al, etc.)
CNT-un	97	0.05	2.6	0.05	0.3
CNT-200	96	1.9	1.5	0.05	0.55
CNT-400	97	0.9	1.4	0.05	0.65
Ru/CNT-un	98	0.05	1.5	0.05	0.4
Ru/CNT-200	98	0.4	1.2	0.0	0.4
Ru/CNT-400	98	0.1	1.3	0.05	0.55

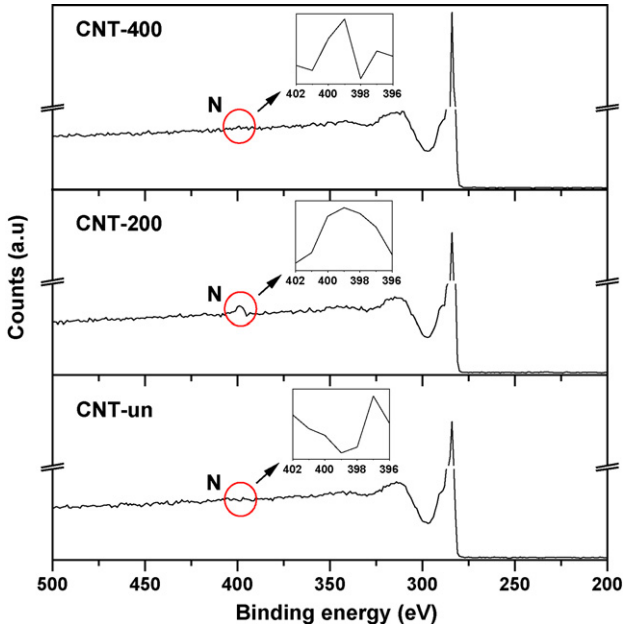

Fig. 1. Survey scans of the different CNTs with XPS before and after nitrogen doping in N_2 MW plasma at 200 and 400 W of the MW power.

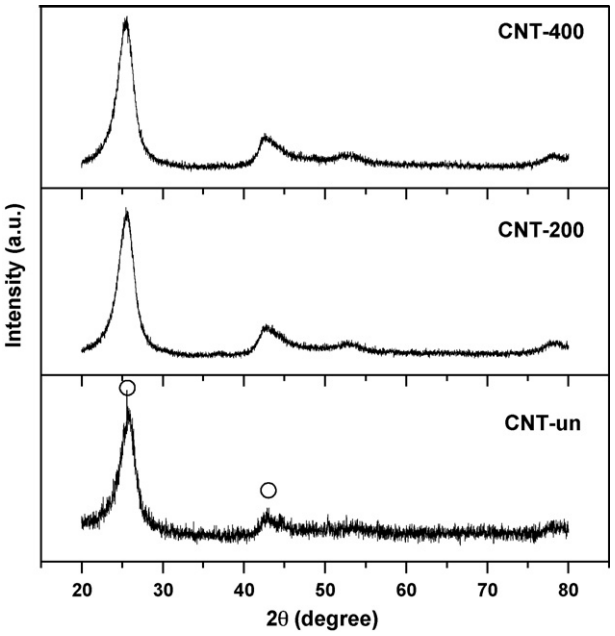

Fig. 3. XRD profiles of the different CNTs before and after nitrogen doping in N_2 MW plasma at 200 and 400 W of the MW power; Cu Kα; (○) graphite.

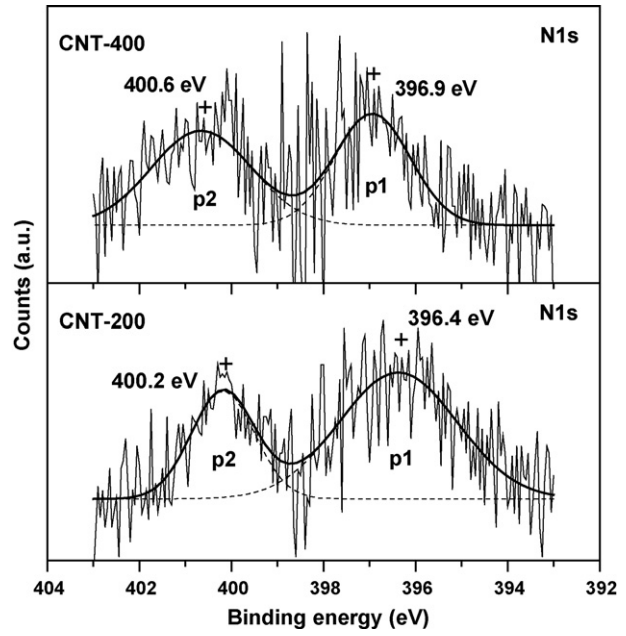

Fig. 2. Binding energy of N1s on the different CNTs after nitrogen doping in N_2 MW plasma at 200 and 400 W of the MW power.

that the amount of the remaining Fe is very low after being soaked in HNO_3 solution.

Fig. 2 shows the narrow scans of N1s of CNT-200 and CNT-400. The N1s signals for CNT-un were masked by the high noise/signal ratio, due to the much low content of nitrogen on the sample. The N1 spectra of CNT-200 and CNT-400 can be fitted into two Gaussian sub-peaks referred as p1 and p2, around 397 and 400 eV, respectively, suggesting two nitrogen species present on N-doped CNTs. The details of fitting results, namely binding energy (BE), full widths at half maximum (FWHM), and area ratio of p1/p2 are given in Table 2. As seen, BE values for CNT-400 are slightly higher than those of CNT-200 but the area ratio of p1/p2 is higher for CNT-200.

The XRD profiles of CNT-un, CNT-200 and CNT-400 are illustrated in Fig. 3. There is no obvious difference between the bulk structure of the CNT samples before and after nitrogen doping, and the main peaks of all the CNTs are similar to those of graphite, which indicates that the employed CNTs are highly graphitized.

The pore size distribution curves of CNT-un, CNT-200 and CNT-400 obtained from N_2 physisorption are shown in Fig. 4. There are only some slight changes of the curves for the three samples. A small decrease in the pore volume is observed at diameter of 2.5–4.0 and 13–15 nm for CNT-200 and CNT-400, suggesting that the N-doping produces some collapse of large pores. The specific surface areas of CNT-un, CNT-200 and CNT-400 are 160, 130 and 140 $m^2\,g^{-1}$, respectively. These changes can be considered insignificant considering the resolution of the adsorption instrument. These results show that the surface texture of CNTs is not changed significantly after nitrogen doping in N_2 MW plasma.

3.2. Characterization of Ru/CNTs

Fig. 5 shows the XPS survey scans of Ru/CNT-un, Ru/CNT-200 and Ru/CNT-400 after reduction in hydrogen at 773 K. In the range of 280–300 eV of BE, the carbon signals are pronounced, the nitrogen signals are weaker and the signals of Ru3d (around 282 eV) are overlapped and masked by those of C1s (around 284 eV). The

Table 2
Results of the deconvolution of XPS spectra of the N1s region.

Samples	p1 (pyridinic nitrogen)		p2 (quaternary nitrogen)		Area ratio of p1/p2
	BE (eV)	FWHM (eV)	BE (eV)	FWHM (eV)	
CNT-200	396.4	3.0	400.2	1.6	2/1
CNT-400	396.9	1.9	400.6	2.6	1/1

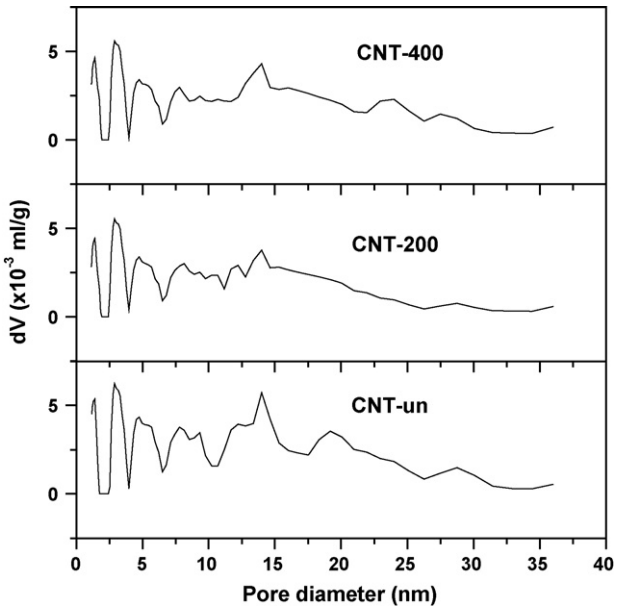

Fig. 4. Pore size distributions of the different CNTs measured before and after nitrogen doping in N_2 MW plasma at 200 and 400 W of the MW power.

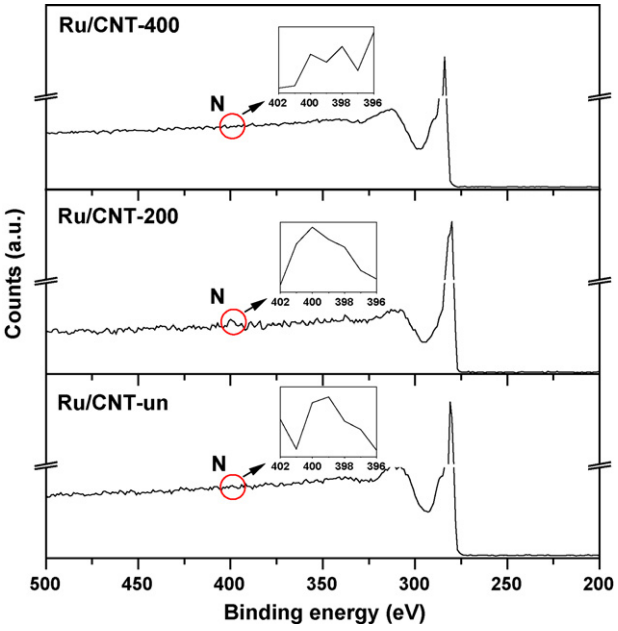

Fig. 5. Survey scans of the different Ru/CNTs with XPS after reduction in hydrogen at 773 K.

Table 3
Dispersion and average size of Ru particles supported on CNTs measured with CO chemisorption.

Samples	Weight (mg)	CO adsorption (μl)	D_{Ru} (%)	d_{Ru} (nm)
Ru/CNT-un	500	138	16	8.6
Ru/CNT-200	450	244	31	4.4
Ru/CNT-400	470	188	23	6.0

corresponding elemental analysis shows that nitrogen contents of Ru/CNT-200 and Ru/CNT-400 are decreased greatly compared with CNTs supports (Table 1). For CNT-200 and CNT-400, nitrogen content is 0.4% and 0.1%, respectively, which is due to further higher temperature treatment during Ru-based catalyst preparation. Additionally, Cl was not observed with XPS on the three Ru/CNTs samples, which suggests that the Cl residues from $RuCl_3$ were removed completely after the calcination and reduction in hydrogen at 773 K [9,12].

Fig. 6A–C shows the TEM photos of Ru particles on Ru/CNT-un, Ru/CNT-200 and Ru/CNT-400 catalysts after reduction at 773 K, respectively. Since Ru loading content was all 0.8 wt.%, it was difficult to find many particles in a single observation. However, based upon the observation of 20 particles, the average size of Ru particles could be evaluated as ca. 15, 5 and 8 nm on supported Ru/CNT-un, Ru/CNT-200 and RuCNT-400 catalysts, respectively. The results show that smaller Ru particle could be obtained on nitrogen doped CNT supports. Furthermore, no Fe particles were found in TEM observation, suggesting they were removed during the pretreatment using 4 M HNO_3 solution to soak the CNTs.

CO chemisorption was used to measure the dispersion of Ru particles (D_{Ru}) and the average size of Ru particles (d_{Ru}) by assuming a surface stoichiometry of CO/Ru = 1. The surface area of Ru metal particles was calculated assuming a Ru surface density of 1.63×10^{19} atoms m^{-2}, and a hemisphere model of a Ru particle which contacts with the CNT surface by its cross section plane. The average size (d_{Ru}) of Ru particles was determined from the CO uptake by the expression $d_{Ru} = 6V/S$, where V and S are the metal volume and the surface area of Ru, respectively [19,20]. The results of D_{Ru} and d_{Ru} of Ru/CNT-un, Ru/CNT-200 and Ru/CNT-400 are listed in Table 3. It is clearly shown that, after nitrogen doping on CNTs, the dispersion of Ru particles is clearly improved.

3.3. Catalytic activity of Ru/CNTs in ammonia decomposition

Fig. 7 shows the rate of ammonia decomposition and turnover frequencies (TOFs) of three Ru/CNT catalysts at 773, 823 and 873 K. Ru is an expensive metal, and from a technological perspective a high rate of ammonia conversion, related to its mass, is a key criterion of the catalyst's performance [15]. However, a scientific understanding is also of importance so the surface activity,

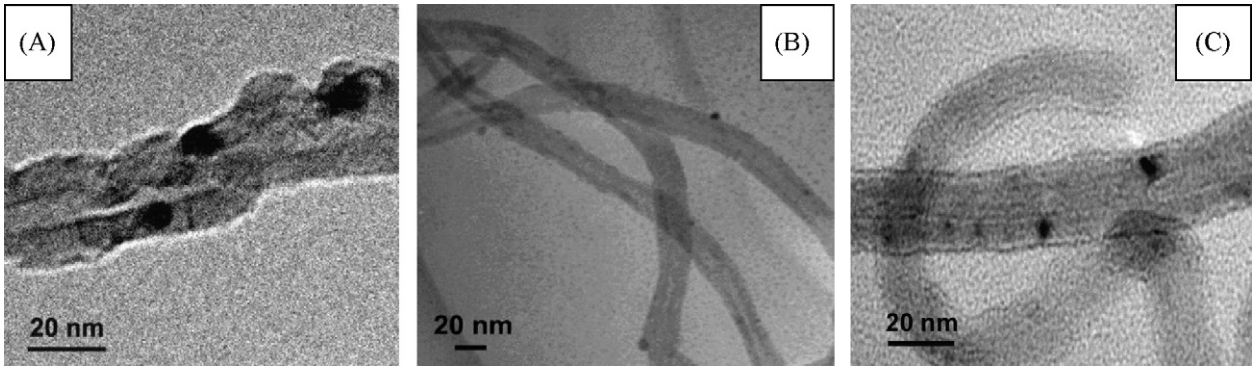

Fig. 6. TEM photographs of Ru particles of the different Ru/CNTs after reduction in hydrogen at 773 K: (A) Ru/CNT-un; (B) Ru/CNT-200; (C) Ru/CNT-400.

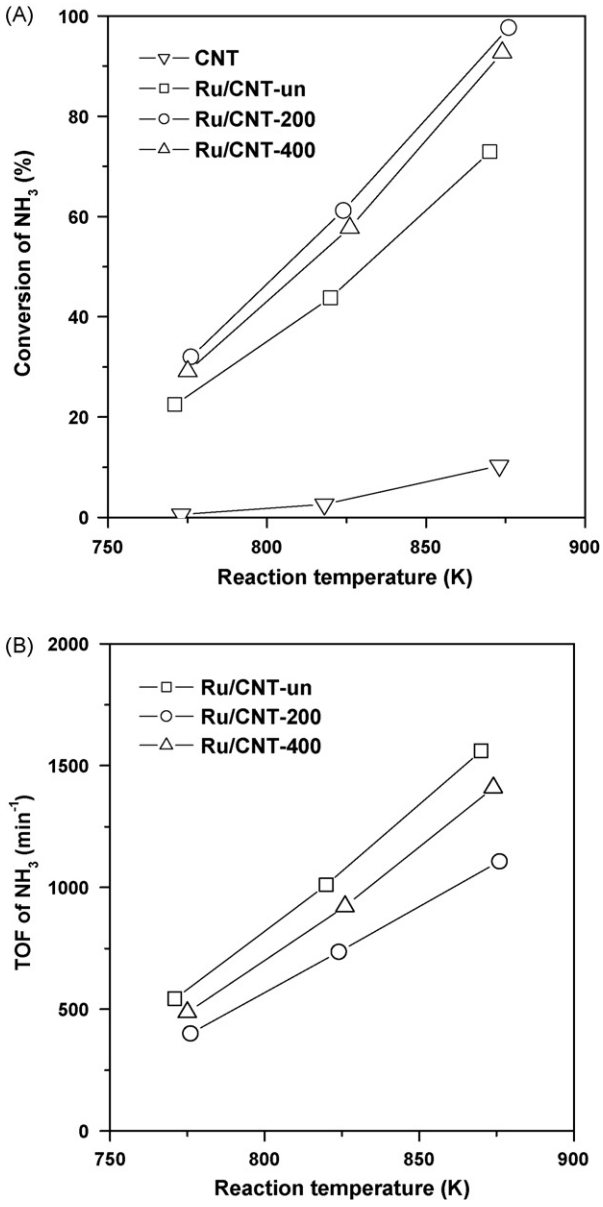

Fig. 7. Conversion (A) and TOF (B) of ammonia at 773–873 K on the different Ru/CNTs.

expressed in turnover frequency (TOF) of ammonia, is also significant. In catalysis, TOF is also called turnover number, and is defined as molecules reacting per active site in unit time. The number of the reacting molecules of ammonia in unit time can be calculated out from the conversion and the flow rate of ammonia at the corresponding reaction temperature and the available number of Ru active sites on the corresponding catalyst can be obtained from the dispersion of Ru atoms measured from CO chemical adsorption as above (Table 3). Additionally, a blank activity test of ammonia decomposition was carried out as the reference on CNTs without loading of Ru after being soaked in 4 M nitric acid (Fig. 7A). It seems that the catalytic behaviors of CNTs (containing 0.05 at.% Fe) at low temperatures can be negligible, however, the catalytic activity of CNTs is increased with the reaction temperature. This number of the converted ammonia on CNTs in the blank activity test has been taken into account when TOF on the different Ru catalysts was calculated (Fig. 7B).

From Fig. 7A, it is seen that ammonia conversion rate increases with increasing temperature. For three catalysts, ammonia conversion shows an order of Ru/CNT-200 > Ru/CNT-400 > Ru/CNT-un. However, from Fig. 7B, the order of TOF values on the three samples is opposite to that of the above reaction rate.

4. Discussion

4.1. Effects of nitrogen doping on the structure of CNTs

Elemental analysis from XPS shows the presence of nitrogen on the surface of CNTs, which indicates that N_2 MW plasma is an effective approach for doping nitrogen atoms on CNTs. However, the plasma power influences the doping temperature and thus affects the nitrogen contents and their chemical states on CNTs. From Table 1, it is seen that CNT-400 has lower nitrogen content, which is due to the high temperature of CNT inducing higher evaporation of nitrogen. In addition, N1s XPS spectra on CNT-200 and CNT-400 show clearly two sub-peaks p1 and p2 around 397 and 400 eV, respectively (Fig. 2). From the literature [21–28], N1s BEs of carbon nitride formed on solid carbon materials were found to be around 398 and 401 eV. The shift of BE in this investigation is ascribed to the different chemical environments for nitrogen atoms in various compounds and the relaxation effect in the measurement process [29–31]. According to the literature [24–27,32–34], p1 can be attributed to the tetrahedral C–N bonding with C in sp^3 hybridization and N in sp^2 hybridization states. The nitrogen atoms in this bonding state are located at the edge of the graphene sheet in the plane of the graphite and are referred to as pyridinic nitrogen [25–27,32]. On the other hand, p2 is assigned to trigonal C–N bonding with both C and N in sp^2 hybridization state. The nitrogen atom substitutes for a carbon atom in the hexagonal graphene sheet. These nitrogen atoms within the graphene sheets are termed as quaternary nitrogen [25–27,32].

For CNT-200 and CNT-400, the area ratio of p1/p2 is different and CNT-200 exhibits higher ratio, suggesting that high doping temperature (associated with higher MW power) favors the formation of quaternary nitrogen and low doping temperature is favorable to the generation of pyridinic nitrogen. Thermal stability of pyridinic nitrogen is usually lower. This result is consistent with the literature [25–27,32]. XRD (Fig. 3) and N_2 physisorption measurements (Fig. 4) show that there was no significant influence of the doped nitrogen on the bulk structure and the surface texture of CNTs. This is probably due to small amount of pyridinic and quaternary nitrogen on CNTs.

4.2. Effects of nitrogen doping on the dispersion of Ru particles

The average Ru particle size on Ru/CNT was obtained from TEM and CO chemisorption. For Ru/CNT-un, TEM observation and CO chemisorption are different, but they are consistent for Ru/CNT-200 and Ru/CNT-400. The difference can be ascribed to the measurement error of the methods. In the comparison of three catalysts, it is seen that Ru particle size follows the same order, Ru/CNT > Ru/CNT-400 > Ru/CNT-200. Thus it is concluded that the dispersion of the Ru particles is significantly improved after nitrogen doping.

Pyridinic nitrogen atoms, located at the edges of the graphene sheets on the surface of CNTs are more easily to contact with metal ions Ru^{3+} adsorbed on the surface of CNTs than the quaternary nitrogen within the graphene sheet in the bulk of CNTs [25,32]. Each pyridinic nitrogen atom in sp^2 hybridization state has an unbonded electron pair, being able to complex the empty orbital of Ru^{3+} as a ligand and anchor the Ru^{3+}, thus hindering agglomeration and surface diffusion of Ru^{3+} and minimizing the sintering of Ru particles across the surface of CNTs at high temperature of calcination and reduction [35]. Table 1 shows that more pyridinic nitrogen are formed on CNT-200 than on CNT-400, the interaction

of CNT-200 with Ru particles is thus stronger and the Ru particles are more resistant to sintering during calcination and reduction in the preparation process.

4.3. Effects of nitrogen doping on the activity of Ru/CNTs

The characterization results (XRD and N_2 adsorption) show that nitrogen doping on CNTs did not induce changes of bulk structure and surface texture of CNTs. However, nitrogen doping introduced different electron states of nitrogen atom and change of Ru dispersion, which will influence catalytic activity of Ru/CNT.

For CNT-un and Ru/CNT-un, XPS measurement shows that the contents of nitrogen in CNT-un and Ru/CNT-un are both about 0.05 at.% (Table 1), which implies that these nitrogen may not originate from the adsorbed nitric acid during soaking process, but from synthesis process of CNTs at high temperatures, otherwise, the content of nitrogen in Ru/CNT-un should be much lower than that in CNT-un because nitric acid can be removed during the calcination and reduction process of Ru/CNT-un at 773 K. Compared with the doped nitrogen in plasma process, the amount of these nitrogen is negligible. On the other hand, all the CNT supports in this work originate from the same CNTs. Therefore, the promoting effects of the doping nitrogen by plasma on the activity of Ru in ammonia decomposition can still be observed despite the existence of these nitrogen.

In general, catalytic activity of Ru-based catalyst will be dependent on dispersion of Ru particle and electron transfer ability. Due to low loading of Ru on CNTs, the binding energies of Ru particles on Ru/CNT-un, Ru/CNT-200 and Ru/CNT-400 could not be detected using XPS. The surface elemental analysis showed that some nitrogen atoms still remain on Ru/CNTs samples after Ru impregnation and reduction in hydrogen at 773 K (Table 1). The remaining surface nitrogen can reduce the surface activity of Ru as a result of electron withdrawal [12–14]. Although oxygen content is higher than nitrogen on Ru/CNTs samples (Table 1), oxygen atoms do not act as the main sites to anchor Ru particles while nitrogen atoms are strongly bounded with Ru and show local electron-drawing interaction [15]. Also, elemental analysis indicates that oxygen content on three catalysts is similar, but nitrogen is quite different. Thus, the activity will be more related to nitrogen. It has been reported that the doping of nitrogen in CNTs can increase the basicity of CNTs, which may be advantageous to electron transfer from CNTs to Ru and increasing the activity of Ru for ammonia decomposition [32]. However, nitrogen is more electronegative than Ru and has an electron-withdrawing effect from Ru atoms [12–16]. The order of TOF on Ru/CNT-un, Ru/CNT-400 and Ru/CNT-200 catalysts in Fig. 7B is the same order of the remaining nitrogen content reflecting more negative effect of electron withdrawal caused by nitrogen on ammonia decomposition.

On the other hand, Ru particles in this investigation are bigger than 2.5 nm, higher dispersion of Ru particles on catalyst surface will be advantageous to promote the activity of Ru/CNTs in ammonia decomposition. Therefore, the activity of Ru/CNTs in ammonia decomposition is closely related to the dispersion of Ru particles. From Table 3, it has shown that Ru dispersion follows an order of Ru/CNT-200 > Ru/CNT-400 > Ru/CNT-un and thus the rate of activity of the three catalysts exhibits the same order as shown in Fig. 7A.

5. Conclusions

Nitrogen doping on CNTs in N_2 MW plasma produced two forms of nitrogen species. One is pyridinic nitrogen at the edge of graphene sheet on the surface of CNTs and the other is quaternary nitrogen within the graphene sheet. The increase of MW power reduced the ratio of pyridinic nitrogen to quaternary nitrogen on CNTs. However, nitrogen doping will not significantly change the bulk structure and the surface texture of CNTs due to low nitrogen content. The dispersion of Ru particles on CNTs can be improved with the increasing content of doped nitrogen ascribed to a stronger interaction of Ru particles with pyridinic nitrogen on the surface of CNTs. The average size of Ru particles decreases with the increase of pyridinic nitrogen content on CNTs. The activity of Ru/CNTs in ammonia decomposition is dependent on the dispersion of Ru particles and amount of nitrogen on the surface of CNTs. Among the three Ru/CNT catalysts prepared in this investigation, Ru/CNT-200 exhibited the highest activity in terms of reaction rate.

References

[1] A.S. Chellappa, C.M. Fischer, W.J. Thomson, Ammonia decomposition kinetics over Ni–Pt/Al_2O_3 for PEM fuel cell applications, Appl. Catal. A 227 (2002) 231–240.
[2] X.K. Li, W.J. Ji, J. Zhao, S.J. Wang, C.T. Au, Ammonia decomposition over Ru and Ni catalysts supported on fumed SiO_2, MCM-41, and SBA-15, J. Catal. 236 (2005) 181–189.
[3] C.S. Song, Fuel processing for low-temperature and high-temperature fuel cells: challenges, and opportunities for sustainable development in the 21st century, Catal. Today 77 (2002) 17–49.
[4] T.J. Schmidt, Z. Jusys, H.A. Gasteiger, R.J. Behm, U. Endruschat, H. Boennemann, On the CO tolerance of novel colloidal PdAu/carbon electrocatalysts, J. Electroanal. Chem. 501 (2001) 132–140.
[5] Y.D. Li, J.L. Chen, Y.N. Qin, L. Chang, Simultaneous production of hydrogen and nanocarbon from decomposition of methane on a nickel-based catalyst, Energy Fuels 14 (2000) 1188–1194.
[6] T.V. Choudhary, C. Sivadinarayana, D.W. Goodman, Production of CO_x-free hydrogen for fuel cells via step-wise hydrocarbon reforming and catalytic dehydrogenation of ammonia, Chem. Eng. J. 93 (2003) 69–80.
[7] L. Li, Z.H. Zhu, Z.F. Yan, G.Q. Lu, L. Rintoul, Catalytic ammonia decomposition over Ru/carbon catalysts: the importance of the structure of carbon support, Appl. Catal. A 320 (2007) 166–172.
[8] L. Li, Z.H. Zhu, G.Q. Lu, Z.F. Yan, S.Z. Qiao, Catalytic ammonia decomposition over CMK-3 supported Ru catalysts: effects of surface treatments of supports, Carbon 45 (2007) 11–20.
[9] S.F. Yin, B.Q. Xu, X.P. Zhou, C.T. Au, A mini-review on ammonia decomposition catalysts for on-site generation of hydrogen for fuel cell applications, Appl. Catal. A 277 (2004) 1–9.
[10] S.F. Yin, B.Q. Xu, C.F. Ng, C.T. Au, Nano Ru/CNTs: a highly active and stable catalyst for the generation of CO_x-free hydrogen in ammonia decomposition, Appl. Catal. B 48 (2004) 237–241.
[11] T.V. Choudhary, D.W. Goodman, CO-free fuel processing for fuel cell applications, Catal. Today 77 (2002) 65–78.
[12] Z.H. Zhong, K. Aika, The effect of hydrogen treatment of active carbon on Ru catalysts for ammonia synthesis, J. Catal. 173 (1998) 535–539.
[13] Z.H. Zhong, K. Aika, Effect of ruthenium precursor on hydrogen-treated active carbon supported ruthenium catalysts for ammonia synthesis, Inorg. Chim. Acta 280 (1998) 183–188.
[14] K. Aika, A. Ohya, A. Ozaki, Y. Inoue, I. Yasmuri, Support and promoter effect of ruthenium catalyst. 2. Ruthenium alkaline-earth catalyst for activation of dinitrogen, J. Catal. 92 (1985) 305–311.
[15] W. Raróg-Pilecka, E. Miśkiewicz, D. Szmigiel, Z. Kowalczyk, Structure sensitivity of ammonia synthesis over promoted ruthenium catalysts supported on graphitised carbon, J. Catal. 231 (2005) 11–19.
[16] C.J.H. Jacobsen, S. Dahl, P.L. Hansen, E. Törnqvist, L. Jensen, H. Topsøe, D.V. Prip, P.B. Møenshaug, I.B. Chorkendorff, Structure sensitivity of supported ruthenium catalysts for ammonia synthesis, J. Mol. Catal. A 163 (2000) 19–26.
[17] P. Serp, M. Corrias, P. Kalck, Carbon nanotubes and nanofibers in catalysis, Appl. Catal. A 253 (2003) 337–358.
[18] H.W. Chen, V. Rudolph, The 3-D structure of polycrystalline diamond film by electron backscattering diffraction (EBSD), Diamond Relat. Mater. 12 (2003) 1633–1639.
[19] J.R. Anderson, Surface of Metallic Catalysts, Academic Press, New York, 1975, p. 107.
[20] G. Nerl, R. Pietropaolo, S. Galvagno, C. Milone, J. Schwank, Characterization of carbon-supported ruthenium–tin catalysts by high-resolution electron-microscopy, J. Chem. Soc., Faraday Trans. 90 (1994) 2803–2807.
[21] J.W. Jang, C.E. Lee, S.C. Lyu, T.J. Lee, C.J. Lee, Structural study of nitrogen-doping effects in bamboo-shaped multiwalled carbon nanotubes, Appl. Phys. Lett. 84 (2004) 2877–2879.
[22] B. Ruelle, A. Peeterbroeck, R. Gouttebaron, T. Godfroid, F. Monteverde, J.P. Dauchot, M. Alexandre, M. Hecq, P. Dubois, Functionalization of carbon nanotubes by atomic nitrogen formed in a microwave plasma Ar^+N_2 and subsequent poly(epsilon-caprolactone) grafting, J. Mater. Chem. 17 (2007) 157–159.
[23] C. Ronning, H. Feldermann, R. Merk, H. Hofsäss, P. Reinke, J.U. Thiele, Carbon nitride deposited using energetic species: a review on XPS studies, Phys. Rev. B 58 (1998) 2207–2215.
[24] G. Beshkov, D.B. Dimitrov, S. Georgiev, D.J. Cheng, P. Petrov, N. Velchev, V. Krastev, XPS spectra of thin CN_x films prepared by chemical vapor deposition, Diamond Relat. Mater. 8 (1999) 591–594.

[25] F. Kapteijn, J.A. Moulein, S. Matzner, H.P. Boehm, The development of nitrogen functionality in model chars during gasification in CO_2 and O_2, Carbon 37 (1999) 1143–1150.
[26] K. Stanczyk, R. Dziembaj, Z. Piwowarska, S. Witkowski, Transformation of nitrogen structures in carbonization of model compounds determined by XPS, Carbon 33 (1995) 1383–1392.
[27] J.W. Liu, S. Webster, D. Carroll, Temperature and flow rate of NH_3 effects on nitrogen content and doping environments of carbon nanotubes grown by injection CVD method, J. Phys. Chem. B 109 (2005) 15769–15774.
[28] J.P. Zhao, Z.Y. Chen, T. Yano, T. Ooie, M. Yoneda, J. Sakakibara, Structural and bonding properties of carbon nitride films synthesized by low energy nitrogen-ion-beam-assisted pulsed laser deposition with different laser fluences, J. Appl. Phys. 89 (2001) 1634–1640.
[29] F. Le Normand, J. Hommet, T. Szörényi, C. Fuchs, E. Fogarassy, XPS study of pulsed laser deposited CN_x films, Phys. Rev. B 64 (2001) 235416-1–235416-15.
[30] L.H. Chan, K.H. Hong, D.Q. Xiao, T.C. Lin, S.H. Lai, W.J. Hsieh, H.C. Shih, Resolution of the binding configuration in nitrogen-doped carbon nanotubes, Phys. Rev. B 70 (2004) 125408-1–125408-7.
[31] C. Morant, J. Andrey, P. Prieto, D. Mendiola, J.M. Sanz, E. Elizalde, XPS characterization of nitrogen-doped carbon nanotubes, Phys. Stat. Sol. A 203 (2006) 1069–1075.
[32] S. van Dommele, K.P. de Jong, J.H. Britter, Nitrogen-containing carbon nanotubes as solid base catalysts, Chem. Commun. 46 (2006) 4859–4861.
[33] S.K. Srivastava, V.D. Vankar, S.D.V. Rao, V. Kumar, Enhanced field emission characteristics of nitrogen-doped carbon nanotube films grown by microwave plasma enhanced chemical vapor deposition process, Thin Solid Film 515 (2006) 1851–1856.
[34] S. Souto, M. Pickholz, M.C. dos Santos, F. Alvarez, Electronic structure of nitrogen–carbon alloys (a-CN_x) determined by photoelectron spectroscopy, Phys. Rev. B 57 (1998) 2536–2540.
[35] H. Clavier, J.L. Petersen, S.P. Nolan, A pyridine-containing ruthenium–indenylidene complex: synthesis and activity in ring-closing metathesis, J. Org. Chem. 691 (2006) 5444–5447.